Bandwidth Control in Acoustically Coupled AlN Contour Mode MEMS Filters

Carlos R. Perez and Gianluca Piazza
Department of Electrical and Systems Engineering,
University of Pennsylvania, Philadelphia, Pennsylvania
Philadelphia, USA
{carlosrp; piazza}@seas.upenn.edu

***Abstract*— This paper reports a novel method to acoustically couple higher order AlN contour mode resonators and engineer wide bandwidth filters by controlling the number of electrodes, the size of the overhang and the spacing between electrodes. By exciting a higher order resonance mode using multiple metal electrodes on one side of the device and picking up the generated signal on the other, the location of the response poles can be engineered to create a broader band, wider than previously achieved with similar AlN contour-mode devices. CAD-level parameters are experimentally shown to set the location of the poles and therefore the bandwidth.**

I. INTRODUCTION

With constantly increasing demands for new and improved electronic products for commercial as well as military applications, there is currently a need for Radio Frequency (RF) filtering devices which are smaller, more energy efficient, CMOS-integrable, high frequency-capable and inexpensive. A technology that combines the advantages of SAW and FBAR devices (performance, CMOS compatibility, on-die multi-frequency devices) is needed in order to integrate more applications into existing devices such as cellular phones and portable computers, and make possible the deployment of new applications such as distributed sensor networks. One technology that satisfies these requirements is the Piezoelectric Contour Mode Micro-Electro-Mechanical Systems Resonator (MEMS CMR) [1].

In particular, Aluminum Nitride (AlN) based MEMS CMR have simultaneously demonstrated high electromechanical coupling (η) and high quality factor (*Q*), and have shown potential for components that can be directly interfaced with 50 Ω RF systems, whereas lithographically defined features can easily provide frequencies between the low MHz to GHz range [2]. CMR operational frequencies are first order independent of film thickness, favoring higher yields. Additionally, a full range of devices, from resonators to switches [3] and sensors [4] can be fabricated using few lithographic masks, and low temperature, post-IC compatible processes.

Wide bandwidth filters are necessary for many types of RF architectures, and filters synthesized by electrically coupling AlN CMRs are limited by material properties to bandwidths of approximately 2.5 %. In this work we develop an analytic model derived from Mason's theory, and demonstrate how the bandwidth limit can be surpassed through the use of acoustically coupled resonators.

II. DEVICE DESIGN AND MODELING

Fig. 1 shows a schematic of a typical 2 port CMR device. The individual fingers are separate conductor paths with alternating polarities sandwiching the piezoelectric film that forms the device's body. The finger width, number, location and polarity are employed to exclusively excite specific overtones in the AlN plate (Fig. 1). Multi-port configurations are built by mechanically cascading two or more CMR devices, in larger arrays of electrodes or "fingers".

The fingers force the resonator to operate in a higher frequency mode by alternating the polarity of contiguous sections of the resonator, causing them to vibrate with opposite phases. Two port devices can be made by alternating the fingers that form the input and output ports, (Fig. 2a), or by placing all electrodes forming one port on one side of the device and physically separating them from those on the other port (Fig. 2b). When the input and output ports of a device are separated, new modes, beyond the fundamental and its overtones, are present. Furthermore, depending on the device configuration and geometry, some of these modes can appear so close to the fundamental to form a pass band response as

978-1-4244-3510-4/09/$25.00 ©2009 IEEE

shown in Fig. 3. These modes can be employed to synthesize wideband acoustically-coupled filters.

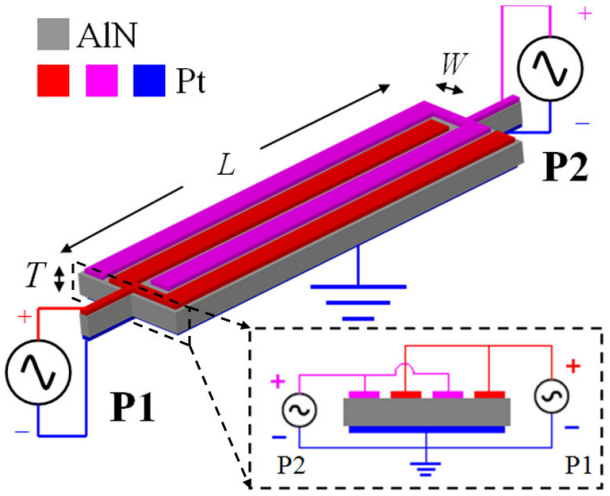

Figure 1. Schematic of a 2-port, 4-finger resonator. Cross section indicates input and output routing.

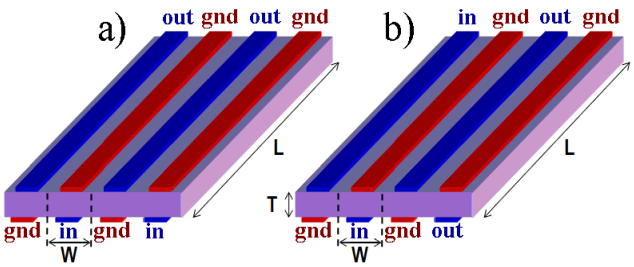

Figure 2. 2-port excitation schemes: alternating input/output (a), and separate input/output (b). *W*, width, is the frequency setting dimension. *T* is the device thickness, and *L* its length. Potentials have ground (gnd) as reference.

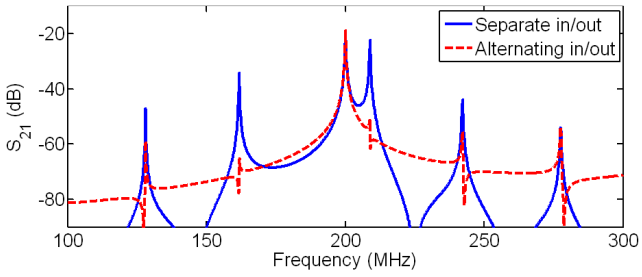

Figure 3. Simulation of alternating vs. separate actuation schemes

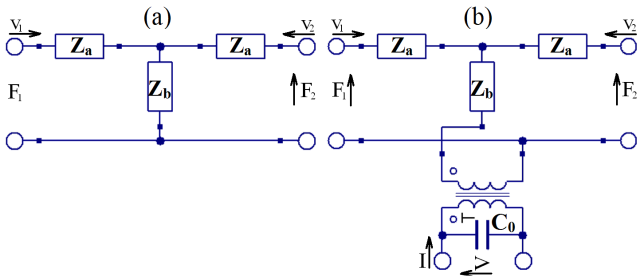

Figure 4. Electromechanical equivalent for (a) passive and (b) piezo-active sections using Mason's model. Left and right ports are mechanical (force/velocity). Bottom port in (b) is electrical (voltage/current)

Mason's model [5] provides the foundation for flexible modeling techniques that are here employed to predict the behavior of these acoustically coupled devices. According to the transmission line concept, Mason proved the equivalence of passive (pure mechanical element) and active (element capable of electromechanical conversion) sections to 2- (Fig. 4a) and 3-port networks (Fig. 4b). Each of the elements of the Mason Model is described by the following equations:

$$\eta = Ed_{31}L, \quad j^* = 1 - \frac{j}{2Q}, \quad R = \frac{j^* TL\sqrt{E\rho}}{\eta^2},$$

$$k = j^*\omega\sqrt{\frac{\rho}{E}}, \quad Z_a = jR\tan\left(\frac{kW}{2}\right), \quad Z_b = \frac{-jR}{\sin(kW)} \quad (1)$$

For the contour mode piezoelectric device operating in a width extensional mode, the values of the series and parallel mechanical impedances, Z_a and Z_b, are thus calculated taking into account that *L*, *W* and *T* are the length, width and thickness of each section, *E* the equivalent Young's modulus of the material stack, and ρ its mass density. The constant d_{31} is the equivalent term of the piezoelectric coefficient that actively excites the resonator into motion.

As with transmission lines, electroacoustic sections of 2 and 3 ports can be handled using matrix representations [6]. When the objective is to cascade mechanically contiguous sections, a transmission matrix form is best suited (i.e. the ABCD form for 2-port networks), since simply multiplying the corresponding matrices yields the desired result. When combining sections that are electrically in parallel, a form similar to the admittance matrix is preferred, since simple matrix addition produces the combined response. In this case each mechanical element can be represented as

$$\begin{bmatrix} v_1 \\ v_2 \\ i \end{bmatrix} = \begin{bmatrix} y_{11} & y_{12} & y_{13} \\ y_{21} & y_{22} & y_{23} \\ y_{31} & y_{32} & y_{33} \end{bmatrix} \begin{bmatrix} F_1 \\ F_2 \\ V \end{bmatrix} \tag{2}$$

Which, by symmetry, is

$$\begin{bmatrix} v_1 \\ v_2 \\ i \end{bmatrix} = \begin{bmatrix} y_{11} & y_{12} & y_{13} \\ y_{12} & y_{11} & y_{13} \\ y_{13} & y_{13} & y_{33} \end{bmatrix} \begin{bmatrix} F_1 \\ F_2 \\ V \end{bmatrix} \tag{3}$$

Here v_1 and v_2, velocities, and F_1 and F_2, forces, for ports 1 and 2, respectively, have been scaled by η^2 in order to eliminate the transformer and simplify the term handling. It can be shown that is possible to express all major terms of the admittance matrix, Y, as a function of known terms y_a and y_b (inverses of Z_a and Z_b), and C_0 as

$$y_{11} = \frac{y_a(y_a + y_b)}{2y_a + y_b}, \quad y_{12} = \frac{-y_a^2}{2y_a + y_b}, \quad y_{13} = \frac{y_a y_b}{2y_a + y_b},$$

$$y_{33} = j\omega C_0 + \left[\frac{1}{2y_a} + \frac{1}{y_b} \right]^{-1} \tag{4}$$

To account for distinct input and output ports, an additional dimension is added, forming a 4-port matrix. These 4-port matrices can then be cascaded to account for the different number and type of fingers. In this way the entire device behavior is model by a very compact 4-port matrix. The polarity of the applied signal (sign of the voltage across the piezoelectric material sandwiched by the two electrodes) is accounted for by changing the sign of the y_{13} or y_{14} terms as needed.

As an example, let us consider the four electrodes, two port device of Fig. 2b. By expressing each distinct electro-acoustic section as a Mason block, and properly connecting them mechanically and electrically, a model of the entire structure can be obtained. This system (Fig. 5) consists of 4 active regions, the fingers, interspaced with 5 passive regions, the spaces between fingers, which are necessary to maintain electrical isolation between signal and ground, and input and output.

The boundary conditions for the mechanical ends of the system consist of an acoustic "short", a zero impedance condition. The interface, often air, is not handled until the final solution matrix of the system is obtained. This offers the additional benefit of easily evaluating loading effects at the extremities without having to re-solve the whole structure.

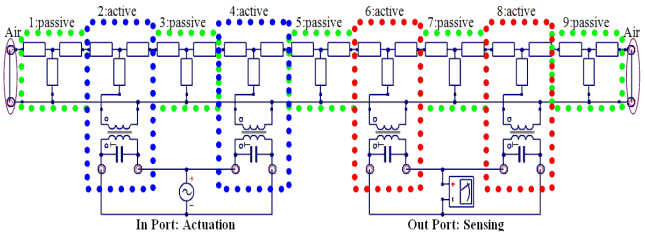

Figure 5. 2-port excitation schemes: alternating input/output (a), and separate input/output (b). W, width, is the frequency setting dimension. T is the thickness, and L length. Potentials have ground (gnd) as reference.

The code iteratively combines the sections, once they are in standard 4x4 matrix form: after solving for the first block and the second, the resulting block is combined with the third, and so on. It accomplishes this by solving the eight linear equations of both matrices to be combined, with the additional constraints: the forces match at the interface, the velocities are opposite, the applied electric field is either input (V_1) or output (V_2), and the currents add into either input (I_1) or output (I_2) current. The reason for this is that there are only two voltages everywhere in the system, and that all currents get lumped into two separate paths.

The experimental results for devices that were previously described using the BVD model [7] were fitted by the implemented Mason model. Dimensional parameters used for the fitting came directly from the design while some other, such as Young's modulus and densities, were taken from material properties tables [8]. Values of Q and C_{ft} (as well as substrate parasitics, when needed) were obtained from the measurement. Fig. 6 shows the good agreement obtained for the device on Fig. 1, which was a 4-finger, 2-port resonator with W of 14 µm and L of 200 µm.

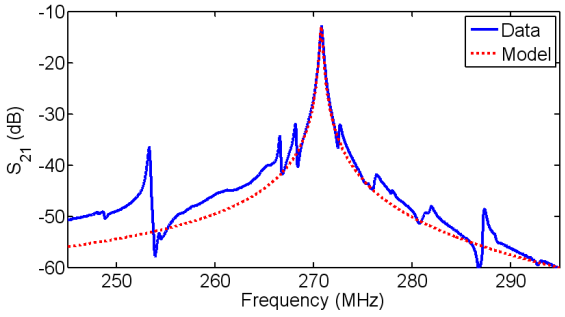

Figure 6. Agreement beteen measured (blue) and modeled (red) response for a a 4-finger, 2-port resonator with W of 14 µm and L of 200 µm.

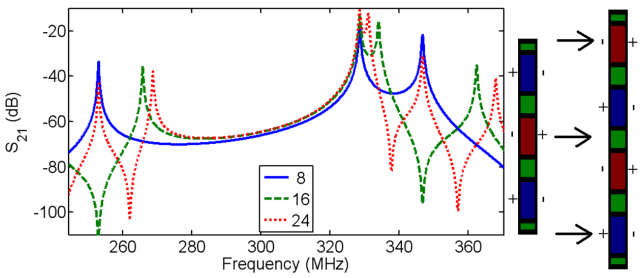

Figure 7. Modeled effect of the number of electrodes.

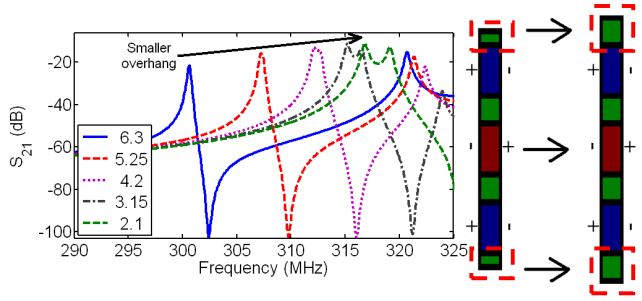

Figure 8. Modeled effect of the overhang size. Legend shows different size of overhang in µm

After verifying the simulation code with known data, the design space was explored to synthesize wide band filters based on acoustically coupled sections. By modifying the parameters of the basic 2-port structure in Fig. 1, the response is engineered to form a passband whose width (in frequency) is determined by the number and size of the electrodes and the size of the AlN overhang, all of which can be set at the layout level.

The effect of increasing the number of electrodes (Fig. 7) was to move some of the modes closer to the fundamental frequency. This can be understood as the presence of more combinations of in-phase and out of phase groups of sections in both the input and the output. Tripling the number of electrodes is observed to double the number of peaks for a given frequency range.

Fig. 8 shows the effect of varying the overhang size (in µm) between two tested values. Besides lowering the fundamental frequency of the device, increasing the overhang size shifts the location of the secondary pole with respect to the fundamental, adding a fine tuning mechanism that is not limited to the discrete number of electrodes.

III. FABRICATION

For this work a standard four mask fabrication process (Fig. 9) previously developed by Piazza *et al.* [9] was employed. The substrates used were 4" single crystal high resistivity (>10 kΩ-cm) silicon wafers. Fig. 9 summarizes the fabrication process flow. Except for Low Stress Nitride (LSN), SiO_2 and AlN film depositions, all processing was performed at the Penn's Wolf Nanofabrication Facility.

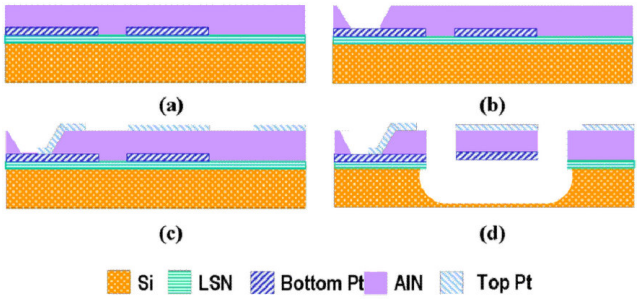

Figure 9. Fabrication process used for the making of AlN resonators and filters. (a) Low stress nitride (LSN) deposition by LPCVD, followed by Pt patterning by lift-off and AlN sputter deposition; (b) Open via access to bottom Pt electrode through AlN; (c) Deposition of top Pt electrode and patterning by lift-off; (d) Cl_2-based dry etching of AlN resonant devices and dry release in XeF2.

A number of different designs (Table I) were fabricated with varying parameters such as number of fingers and overhang size, in order to validate the effects predicted by the analytical model. Fig. 10 shows an SEM of device 11-11 with electrode polarities and overhang marked.

TABLE I. FABRICATED DEVICES

	Device				
	15-21	***10-01***	***10-11***	***11-01***	***11-11***
Actuation type:	Interspaced	Separate	Separate	Separate	Separate
Finger number:	8	8	8	24	24
Finger width:	40 µm	40 µm	40 µm	14 µm	14 µm
Overhang size:	Small	Small	Large	Small	Large

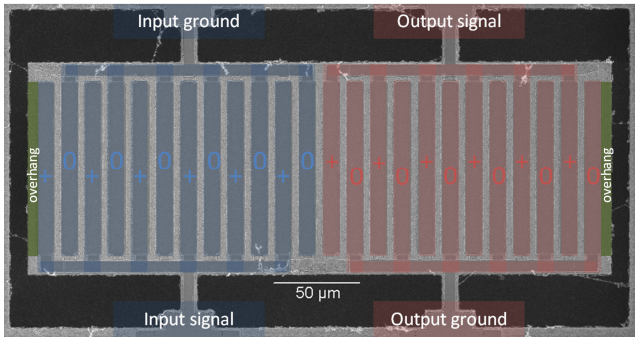

Figure 10. SEM 11-11, a 24-finger 2-port filter with a 6.3 µm overhang.

IV. Experimental Results

The measured response (Fig. 11) of devices for which the number of electrodes was varied fits well with the model's predictions (Fig. 7). The modes in device 10-01 (8 fingers) are separated by ~ 10% of the fundamental frequency. The dip or ripple between them, due to decoupling of the modes, makes generating a practical passband between them impossible. However, device 11-01 (24 fingers) has a smaller bandwidth and a lower ripple.

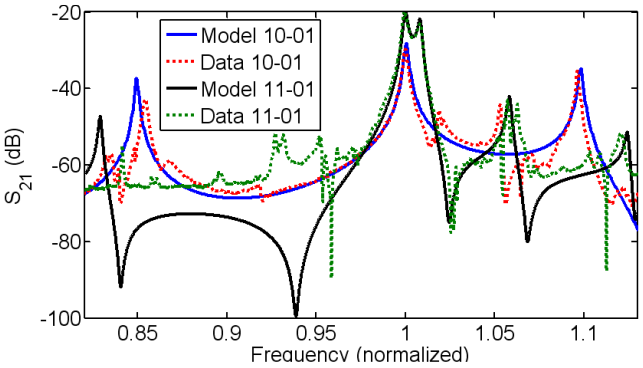

Figure 11. Data and fitted models for 10-01 (8 fingers) and 11-01 (24 fingers) devices. Frequency is normalized to allow overlapped view.

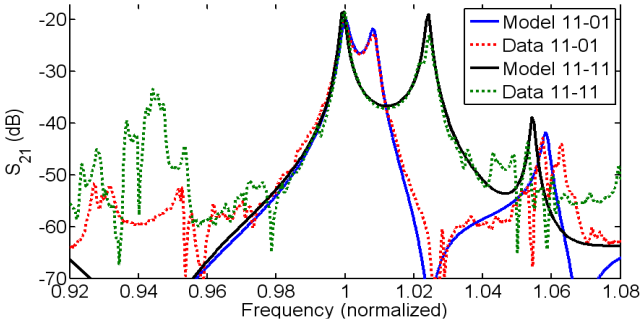

Figure 12. Data and fitted models for 11-01 (2.1 µm overhang) and 11-11 (6.3 µm overhang). Frequency is normalized to allow overlapped view.

A similar comparison between devices 11-01 and 11-11 (Fig. 12) confirms the model's prediction in regards to the effect of overhang size on pole location (Fig. 8). These two devices are identical except for their overhang sizes, 2.1 µm and 6.3 µm, respectively. However, this small difference causes the secondary mode to appear much closer to the fundamental, radically affecting the device's bandwidth.

As for device 11-01, device 11-11 can be matched using an LC network, yielding a filter with a bandwidth of 3.2 %. There is still some ripple, but it is limited to ~ 2 dB. As predicted by the Mason Model, Insertion Loss (IL) increased with designed bandwidth. The reason for this is the decoupling between the two modes that form the band as the frequency difference between them increases. Achieving higher electromechanical coupling through improvements in the piezoelectric material's quality is predicted to thus decrease IL and ripple even for bandwidth in excess of 3 %.

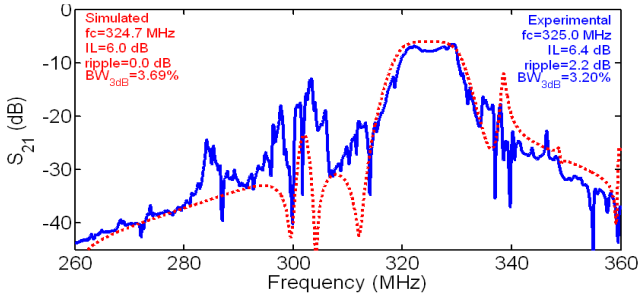

Figure 13. Matched data (blue) and modeled (red) performance of device 11-11. L-C matching networks used had values of L=347 nH and C=126 fF.

A higher Q would also improve IL, but at the expense of ripple, since a higher quality factor would sharpen the individual peaks and increase the decoupling between them.

V. Conclusions

We have presented a method of bandwidth control in acoustically-coupled Aluminum Nitride Contour Mode filters, and accurately predicted the device behavior using an extended Mason's model. The working principle of the simulation technique can also be extended to any other piezoelectric material and, with some modification, to devices operating in different modes. The fabricated devices exhibited bandwidths up to 3.2%, the highest for AlN CMR.

Acknowledgment

The authors would like to thank all the members of Penn's Micro and Nano Systems Laboratory and the staff at the Wolf Nanofabrication Facility.

References

[1] G. Piazza, P.J. Stephanou, and A.P. Pisano, "Piezoelectric Aluminum Nitride Vibrating Contour-Mode MEMS Resonators," Journal of Microelectromechical Systems, Vol 15, pp. 1406-1418, June 2006.

[2] P.J. Stephanou and A.P. Pisano, "GHZ higher order contour mode ALN annular resonators," Micro Electro Mechanical Systems, 2007. MEMS. IEEE 20th International Conference, January 2007.

[3] N. Sinha, R. Mahameed C. Zuo, M.B. Pisani, C.R. Perez, and G. Piazza, "Dual-Beam Actuation of Piezoelectric AlN RF MEMS Switches Integrated with AlN Contour-Mode Resonators," 2008 Solid State Sensor, Actuator and Microsystems Workshop (Hilton Head 2008): pp. 22-25, June 2008.

[4] M. Rinaldi *et al*., " Gravimetric Chemical Sensor Based on the Direct Integration of SWNT's on AlN Contour Mode MEMS Resonators," 2008 IEEE International Frequency Control Symposium, pp. 443-448, May 2008.

[5] W.P. Mason, Electromechanical transducers and wave filters, 2nd ed. New York: Van Nostrand, 1948

[6] J.H.B. Deane, and G.G. Johnstone, "Matrix equations for the relations between two-port parameters". International Journal of Electronics, Vol 73, pp. 141 January 1992.

[7] C. Zuo, N. Sinha, M.B. Pisani, C.R. Perez, R. Mahameed and G. Piazza, "Channel-Select RF MEMS Filters Based On Self-Coupled AlN Contour-Mode Piezoelectric Resonators," in 2007 IEEE International Ultrasonics Symposium: pp. 1156-1159. October 2007

[8] A.F. Wright, "Elastic properties of zinc-blende and wurtzite AlN, GaN, and InN," Journal of Applied Physics,.Vol 82, pp. 2833-2839 June 1997

[9] G. Piazza, P.J. Stephanou, J.M. Porter, M.B.J. Wijesundara and A.P. Pisano, "Low motional resistance ring-shaped contour-mode aluminum nitride piezoelectric micromechanical resonators for UHF applications," Micro Electro Mechanical Systems, 2005. MEMS. IEEE 20th International Conference, pp. 20-23, January 2005